Localized FWI for time-lapse monitoring

Colton Kohnke & Paul Sava, Center for Wave Phenomena, Colorado School of Mines

SUMMARY

Full waveform inversion of seismic data requires building the gradient of an objective function from the forward and adjoint wavefields to update the model (Tarantola, 1984; Symes, 2007; Pratt, 1999). After each model update, wavefields need to be recomputed for the next iteration. Typical models are large and computing wavefields is computationally expensive. For time-lapse applications, the model is expected to change only in a local region, therefore much of the computing time is wasted in regions where the model does not change. The technique described in this paper outlines a process to localize the forward and adjoint wavefield propagation to a local domain such that the wavefields simulated locally are exact compared with those simulated in the full domain. The gradient of the objective function is also accurately built inside the local domain. The wavefields and gradient in each iteration are computed locally at a cost orders of magnitude lower than in the full domain, enabling more computationally efficient inversions.

INTRODUCTION

As geophysical problems get larger, our ability to compute solutions efficiently depends on computation speed, and on the efficiency of the code employed. While the first factor depends on hardware advances, the second is more problem-dependent. An example is time-lapse full waveform inversion (FWI) (Virieux and Operto, 2009; Tarantola, 1984; Symes, 2007; Pratt, 1999). In this problem, seismic surveys are repeated multiple times, typically after injection or production, followed by iterative inversion to infer model changes between the baseline and each subsequent surveys. The model update at each iteration is computed from the gradient of an objective function, which is simply the cross-correlation of forward and adjoint wavefields, as in RTM imaging. The adjoint wavefield is computed using the data difference at the receivers as its source term. After each model update, the forward and adjoint wavefields must be recomputed to build the gradient for the next model update. In general, these models are large and computing wavefields is computationally expensive. This problem is further exaggerated by the fact that for time-lapse applications the model is expected to change in a localized region of interest, so much of the time spent simulating waves is wasted.

The technique described in this paper outlines a process to localize wavefield propagation and build gradients inside a small local domain at lower computational cost than using the full model. This is accomplished by using localization techniques (Vasmel and Robertsson, 2016; Broggini et al., 2017; Willemsen et al., 2016) that essentially move the sources and receivers to the local domain of interest. Boundary conditions on the local domain are applied such that wavefields simulated cheaply in the local domain are the same as if they were computed using the full computational domain. The computational domain is thus restricted to the space of interest, making wavefields simulations less expensive.

Exact localized wavefields were introduced by van Manen et al. (2007) who explore perturbed scattering problems to show exact reconstruction for a local domain. Vasmel and Robertsson (2016) and Broggini et al. (2017) expand the theory with time-domain boundary condition on the local domain to exactly reproduce wavefields inside and show applications to seismic imaging. Willemsen et al. (2016) and Willemsen and Malcolm (2016) show boundary conditions in the frequency domain and FWI applied to updating salt boundaries. The time-lapse FWI case in the frequency domain is shown by Malcolm and Willemsen (2016). In this paper we show how the forward and adjoint wavefields can be localized in the time-domain, and how local gradients are built for time-lapse FWI.

THE VECTOR-ACOUSTIC OPERATOR

Consider the first-order vector-acoustic wave equations

$$\rho \frac{\partial \mathbf{v}}{\partial t} + \nabla p = \mathbf{f} \tag{1}$$

$$\frac{1}{\rho c^2} \frac{\partial p}{\partial t} + \nabla \cdot \mathbf{v} = q, \tag{2}$$

which couple particle velocity $\mathbf{v}(\mathbf{x}, t)$ and pressure $p(\mathbf{x}, t)$ from a dipole source $\mathbf{f}(\mathbf{x}, t)$ and a monopole source $q(\mathbf{x}, t)$. The wavefields propagate in a medium with spatially variable density $\rho(\mathbf{x})$ and velocity $c(\mathbf{x})$. The vector-acoustic equations are solved iteratively using finite-differences on a staggered grid in space and time, similar to a Yee lattice in electromagnetics (Yee, 1966). The pressure sits on the main grid at integer timesteps and the particle velocity is shifted in space and exists at half timesteps. The equations are solved in a leapfrog scheme: particle velocity is derived from the preceding pressure, and pressure is derived from the preceding particle velocity. A layout of the pressure and particle velocity is shown in Figure 1.

We can use the system of equations 1 and 2 to define a linear operator $\mathbf{L}$

$$\mathbf{L}\mathbf{m} = \mathbf{d}_s. \tag{3}$$

The forward wave propagation operator $\mathbf{L}$, model $\mathbf{m}$,

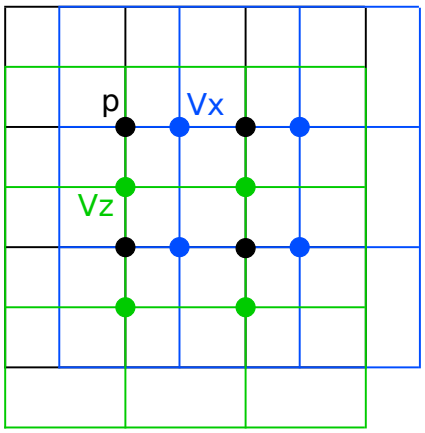

Figure 1: 2D finite-difference grids for equation 1. The pressure grid is shown in black. The grid for the x-component of particle velocity is shown in blue and is shifted by $dx/2$. The z-component of particle velocity is shown in green and is shifted by $dz/2$. In 3D, the y-component of particle velocity is shifted by $dy/2$. Furthermore, the particle velocity grids are shifted from the pressure grid in time by $dt/2$.

and data at the source locations $\mathbf{d}_s$ are defined as

$$\mathbf{L} = \begin{bmatrix} \frac{\rho}{\Delta t}\mathbf{F} & \mathbf{G} \\ \mathbf{D} & \frac{1}{\rho c^2 \Delta t}\mathbf{F} \end{bmatrix}, \mathbf{m} = \begin{bmatrix} \mathbf{v} \\ p \end{bmatrix}, \text{ and } \mathbf{d}_s = \begin{bmatrix} \mathbf{f} \\ q \end{bmatrix}. \quad (4)$$

$\mathbf{G}$ is a diagonal operator with gradient (∇) entries, $\mathbf{D}$ is a diagonal operator with divergence ($\nabla\cdot$) entries, and $\mathbf{F}$ is the operator that performs the finite-difference time derivative of the particle velocity and pressure wavefields. The system is solved for the model $\mathbf{m}$ forward in time by propagating the data at the source locations $\mathbf{d}_s$. The resulting wavefield $\mathbf{m}$ is the state variable needed for imaging. The model at receiver locations $\mathbf{m}_r$ is found by restricting the model wavefields to the receivers. The adjoint wavefield is found using the adjoint of the forward operator $\mathbf{L}^\dagger$

$$\mathbf{m}_r = \mathbf{L}^\dagger \mathbf{d} \quad (5)$$

to solve for the data given the model at the receiver locations. $\mathbf{L}^\dagger$ is the adjoint of the wave propagation operator $\mathbf{L}$ and is defined as

$$\mathbf{L}^\dagger = \begin{bmatrix} \frac{\rho}{\Delta t}\mathbf{F}^\dagger & \mathbf{D}^\dagger \\ \mathbf{G}^\dagger & \frac{1}{\rho c^2 \Delta t}\mathbf{F}^\dagger \end{bmatrix}. \quad (6)$$

$\mathbf{D}^\dagger$, $\mathbf{G}^\dagger$ and $\mathbf{F}^\dagger$ are the adjoint of the corresponding operators. $\mathbf{D}^\dagger$ describes the negative gradient operator and $\mathbf{G}^\dagger$ describes the negative divergence operator. This system is solved for the data $\mathbf{d}$ wavefields in reverse time. This wavefield is restricted spatially to obtain the data at the source $\mathbf{d}_s$. An image can then be formed using the zero-lag crosscorrelation of the state and adjoint variables. The FWI gradient is computed in the same way, but the adjoint wavefield is propagated using the residual between the observed and predicted wavefields at the receiver locations ($\mathbf{m}_r = \mathbf{m}_r^{\text{obs}} - \mathbf{m}_r^{\text{pre}}$).

WAVEFIELD LOCALIZATION

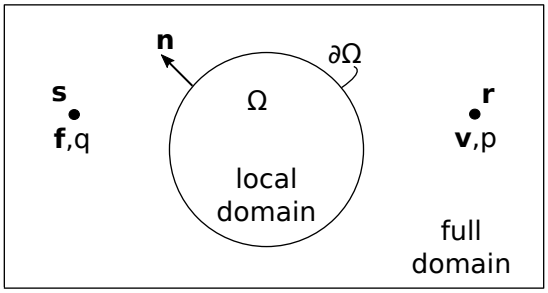

Figure 2: Wavefields generated from the source $\mathbf{s}$ are obtained at the receivers $\mathbf{r}$. The domain Ω is the region of interest where local wavefields are simulated. Ω has the boundary surface $\partial\Omega$ and unit normal $\mathbf{n}$.

Consider the schematic geometry in Figure 2. Using equations equation 3 and 5 we can compute the forward and adjoint wavefields between the sources and receivers and obtain a gradient to update the physical model. Assuming that perturbations only occur in the region Ω, Vasmel and Robertsson (2016) state that we can localize the wavefields with appropriate boundary conditions on $\partial\Omega$ obtained from Rayleigh's Reciprocity Theorem (de Hoop, 1995). If the pressure and particle velocity wavefields are known on $\partial\Omega$ in the full domain, sources on $\partial\Omega$ can be derived such that the wavefields are confined to Ω and are equivalent to those computed in the large domain. In order to localize, we use the forward and adjoint operators to simulate the wavefields on $\partial\Omega$ in the full domain. The localized sources on $\partial\Omega$ are defined as

$$\bar{\mathbf{d}}_{\partial\Omega} = \mathbf{N}\mathbf{m}_{\partial\Omega}. \quad (7)$$

The operator $\mathbf{N}$ acts on $\mathbf{m}_{\partial\Omega}$, the measured wavefields on $\partial\Omega$ in the full domain, to give the new source terms $\bar{\mathbf{d}}_{\partial\Omega}$ on $\partial\Omega$. $\mathbf{N}$ is defined as

$$\mathbf{N} = \begin{bmatrix} 0 & \mathbf{n} \\ \mathbf{n}\cdot & 0 \end{bmatrix} \quad (8)$$

where $\mathbf{n}$ is the outward pointing unit normal of $\partial\Omega$. $\mathbf{N}$ creates $\bar{\mathbf{d}}_{\partial\Omega}$ by swapping the measured wavefields on $\partial\Omega$ based on the normal,

$$\bar{\mathbf{d}}_{\partial\Omega} = \begin{bmatrix} \bar{\mathbf{f}} \\ \bar{q} \end{bmatrix} = \begin{bmatrix} \mathbf{n}p \\ \mathbf{n}\cdot\mathbf{v} \end{bmatrix}. \quad (9)$$

A similar process can be applied to the adjoint. Using the source terms $\mathbf{d}_{\partial\Omega}$ on $\partial\Omega$ in the full domain, equation 5, new adjoint sources are defined as

$$\mathbf{N}\mathbf{d}_{\partial\Omega} = \bar{\mathbf{m}}_{\partial\Omega}. \quad (10)$$

Here $\mathbf{d}_{\partial\Omega}$ is the measured adjoint wavefields on $\partial\Omega$ in the full domain and $\bar{\mathbf{m}}_{\partial\Omega}$ is the new source term on $\partial\Omega$. Substituting these quantities into the forward and

adjoint equations yield

$$\begin{aligned} \mathbf{Lm} &= \bar{\mathbf{d}}_{\partial\Omega} \\ \bar{\mathbf{m}}_{\partial\Omega} &= \mathbf{L}^{\dagger}\mathbf{d} \end{aligned} \tag{11}$$

as the linear systems to solve for the localized forward and adjoint wavefields. We can use the localized wavefields to solve for the proper froward/adjoint pair (equations 3 and 5) inside Ω.

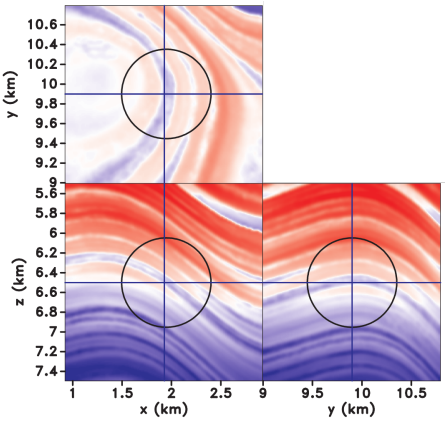

Figure 3: Subset of the SEAM velocity model used for the full domain simulations. The local domain boundary $\partial\Omega$ is highlighted in black.

To illustrate this concept of localization, consider a 200^3 gridpoints subset of the SEAM model and a 100^3 gridpoints subdomain centered around a 0.90km radius sphere (Ω), Figure 3. The large velocity model is the full domain and the smaller velocity model is the local domain. The local domain is 8 times smaller than the full domain, which is indicative of 8 times speedup for wavefield propagation. The smaller the local domain, the higher the speedup.

Figure 4 shows the comparison of the forward operator in the full and local domains for the pressure wavefields. The wavefield reconstructed inside Ω matches the one computed in the full domain. Similarly, the adjoint pressure wavefields in the full and local domain are shown in Figure 5. The adjoint wavefields in the local domain also match inside the local domain as if they were computed in the full domain. The boundaries of the local domain cancel out the wavefields and confine them to propagating inside $\partial\Omega$ for both forward and the adjoint wavefields.

APPLICATION TO FWI

This process of wavefield localization essentially moves sources and receivers to an interior surface $\partial\Omega$ in a process similar to redatuming. The derived forward and adjoint sources form the boundary condition on Ω for the local tomography problem. If the velocity model inside Ω changes, the boundary condition cancel out the

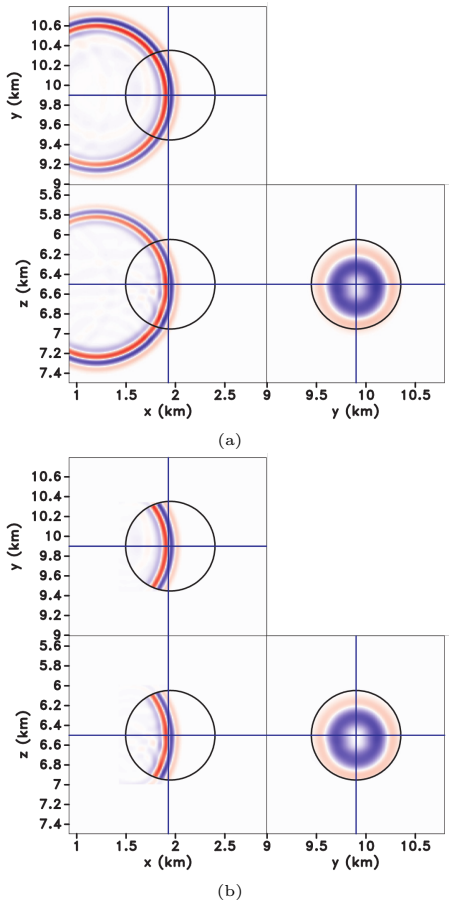

Figure 4: The forward pressure wavefields in the (a) full domain and (b) local domain.

wavefields that propagate in the original model, leaving the scattered wavefields to propagate outside of Ω. This implies that once the wavefields are localized, all of the operations that are required for FWI can be completed using Ω.

Consider a velocity model that has a perturbation confined to Ω, simulating the time-lapse change in the model (Figure 6). The gradient of the objective function is built by crosscorrelation of the localized forward and adjoint wavefields. The forward state variable remains the same as before, based on the forward operator in the local domain. For the adjoint wavefield we relocate the observed wavefields to the region of interest and take the data difference with the predicted wavefields on $\partial\Omega$. This wavefield difference is then propagated using the adjoint equations. Once the observed and predicted wavefields are moved to $\partial\Omega$, the full domain can be ignored because the localized forward operator computes the scattered wavefield on $\partial\Omega$. Figure 7 shows the result of computing the pressure gradient in the full and the local domains. Since the wavefields are accurately localized, the gradients are also localized, and the full and local domain solutions match.

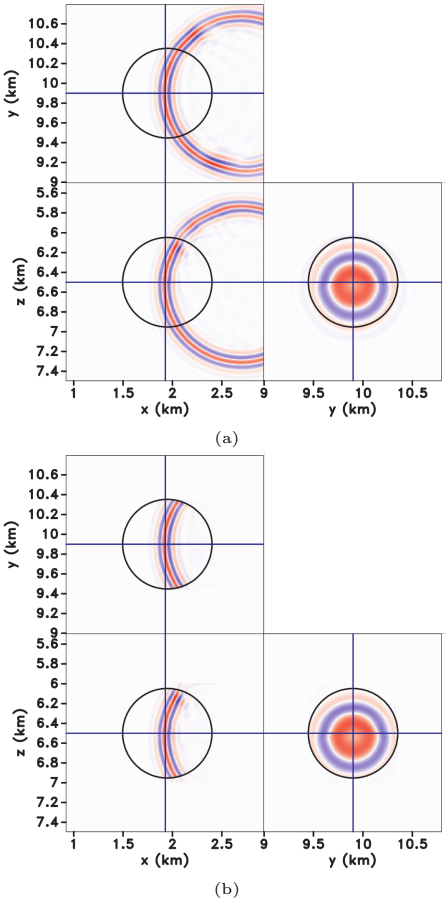

Figure 5: The adjoint pressure wavefields in the (a) full domain and (b) local domain.

CONCLUSION

Time-lapse seismic FWI can be computationally expensive due to the size of the models used for wavefield propagation. We propose a method to localize the forward and adjoint wavefields required by FWI to compute gradients at significantly lower computational cost (up orders of magnitude in 3D) in a local domain. The localization is enabled by boundary condition derived from Rayleigh's Reciprocity Theorem. The wavefields and gradients in the local domain match exactly their counterparts computed in the full model.

ACKNOWLEDGEMENTS

We thank the sponsors of the Center for Wave Phenomena, whose support made this research possible. The synthetic examples in this paper use the Madagascar open-source software package Fomel et al. (2013) freely available from `http://www.ahay.org`.

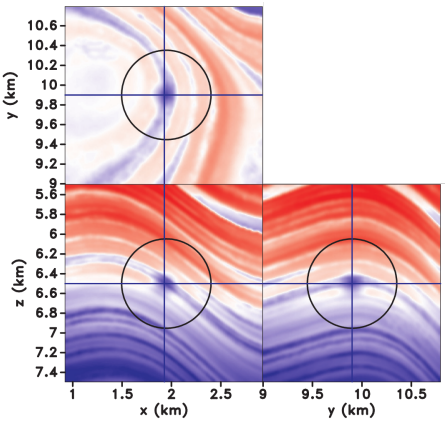

Figure 6: True velocity model for the construction of the observed wavefields at receivers. The boundary of the local domain is highlighted in black.

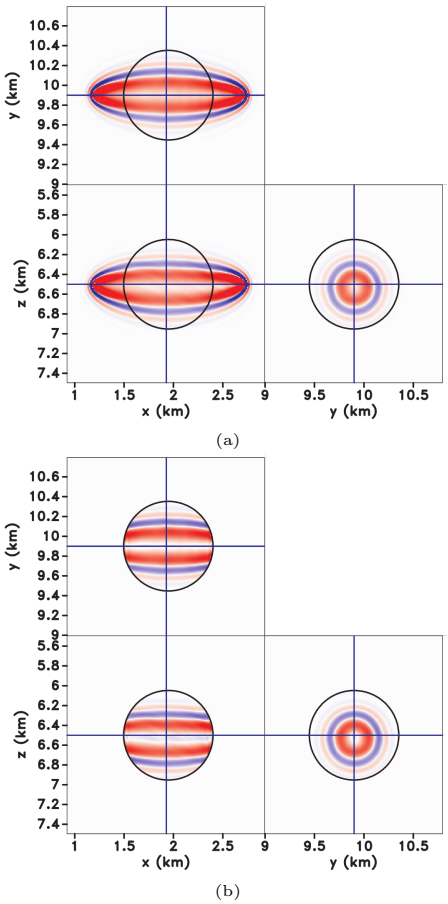

Figure 7: Gradient of objective function built from the crosscorrelation of forward and adjoint pressure wavefields in (a) the full domain and (b) the local domain.

REFERENCES

Broggini, F., M. Vasmel, J. O. A. Robertsson, and D.-J. van Manen, 2017, Immersive boundary conditions: Theory, implementation, and examples: Geophysics, **82**, T97–T110.

de Hoop, A. T., 1995, Handbook of radiation and scattering of waves: Acoustic waves in fluids, elastic waves in solids, electromagnetic waves: Academic Press.

Fomel, S., P. Sava, I. Vlad, Y. Liu, and V. Bashkardin, 2013, Madagascar: open-source software project for multidimensional data analysis and reproducible computational experiments: Journal of Open Research Software, **1**, e8.

Malcolm, A., and B. Willemsen, 2016, Rapid 4D FWI using a local wave solver: The Leading Edge, **35**, 1053–1059.

Pratt, R. G., 1999, Seismic waveform inversion in the frequency domain, Part 1: Theory and verification in a physical scale model: Geophysics, **64**, 888–901.

Symes, W. W., 2007, Reverse time migration with optimal checkpointing: Geophysics, **72**, SM213–SM221.

Tarantola, A., 1984, Inversion of seismic reflection data in the Acoustic Approximation: Geophysics, **49**, 1259–1266.

van Manen, D.-J., J. O. A. Robertsson, and A. Curtis, 2007, Exact wave field simulation for finite-volume scattering problems: The Journal of the Acoustical Society of America, **122**, EL115–EL121.

Vasmel, M., and J. O. A. Robertsson, 2016, Exact wavefield reconstruction on finite-difference grids with minimal memory requirements: Geophysics, **81**, T303–T309.

Virieux, J., and S. Operto, 2009, An overview of full-waveform inversion in exploration geophysics: Geophysics, **74**, WCC1–WCC26.

Willemsen, B., and A. Malcolm, 2016, Coupling a local elastic solver to a background acoustic model to estimate phase variation: SEG Technical Program Expanded Abstracts 2016, Society of Exploration Geophysicists, 3945–3949.

Willemsen, B., A. Malcolm, and W. Lewis, 2016, A numerically exact local solver applied to salt boundary inversion in seismic full-waveform inversion: Geophysical Journal International, **204**, 1703–1720.

Yee, K. S., 1966, Numerical solution of initial boundary value problems involving Maxwell's equations in isotropic media: IEEE Transactions on Antennas and Propagation, **14**, 302–307.